Electronic Supplementary Information (ESI)

Physicochemical Insights into Semiconductor Properties of a Semitransparent Tantalum Nitride Photoanode for Solar Water Splitting

Tomohiro Higashi,*[a] Hiroshi Nishiyama,[b] Yuriy Pihosh,[b] Kaisei Wakishima,[c] Yudai Kawase,[d] Yutaka Sasaki,[d] Akira Nagaoka,[c,e] Kenji Yoshino,[c] Kazuhiro Takanabe,[d] and Kazunari Domen*[b,f]

[a] *Institute for Tenure Track Promotion, University of Miyazaki, 1-1 Gakuen-kibanadai-nishi, Miyazaki, 889-2192, Japan.*
[b] *Office of University Professors, The University of Tokyo, 2-11-16 Yayoi, Bunkyo-ku, Tokyo, 113-8656, Japan.*
[c] *Electrical and Electronic Engineering Program, Faculty of Engineering, University of Miyazak, 1-1 Gakuen-kibanadai-nishi, Miyazaki, 889-2192, Japan*
[d] *Department of Chemical System Engineering, School of Engineering, The University of Tokyo, 7-3-1 Hongo, Bunkyo-ku, Tokyo, 113-8656, Japan*
[e] *Research Center for Sustainable Energy & Environmental Engineering, University of Miyazaki, 1-1 Gakuen-kibanadai-nishi, Miyazaki, 889-2192, Japan*
[f] *Research Initiative for Supra-Materials, Shinshu University, 4-17-1 Wakasato, Nagano, 380-8533, Japan*

*E-mails: domen@chemsys.t.u-tokyo.ac.jp , t_higashi@cc.miyazaki-u.ac.jp

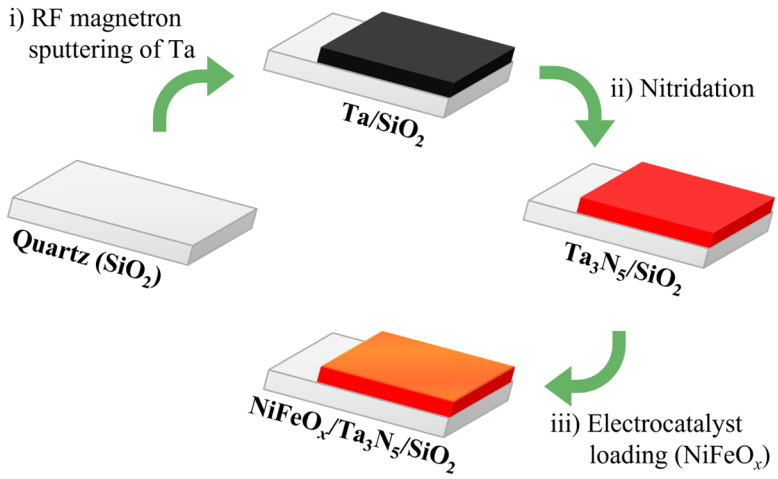

Figure S1. Schematic illustration of the preparation of $NiFeO_x/Ta_3N_5/SiO_2$ thin films.

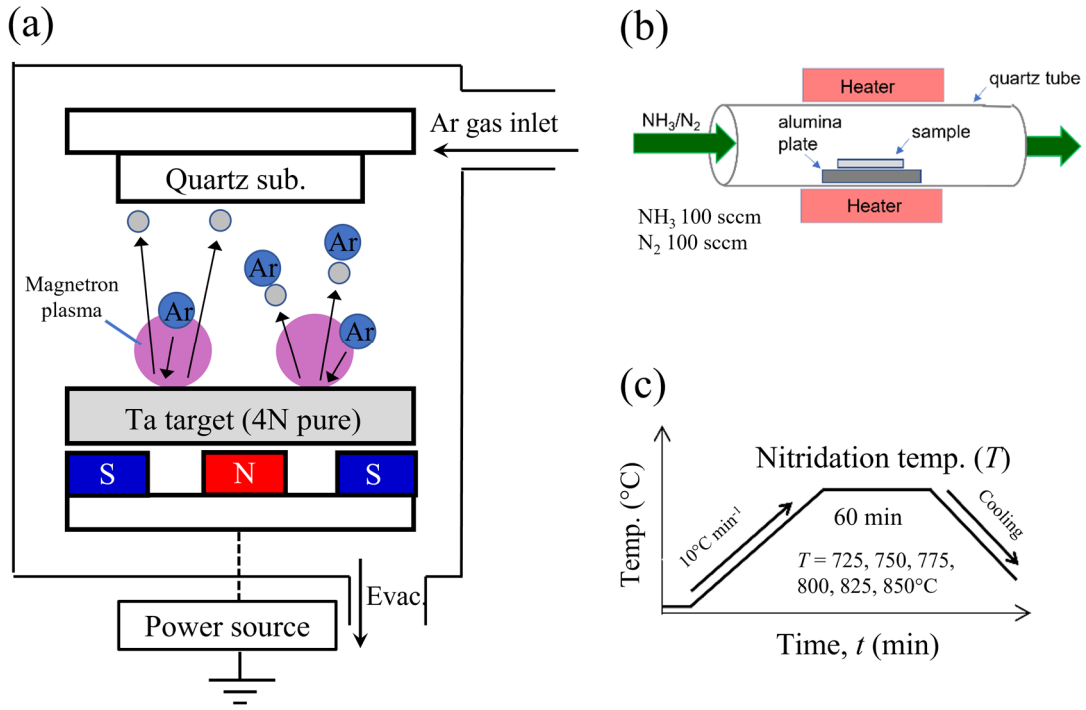

Figure S2. Fabrication process of Ta_3N_5 thin film on double-side polished quartz insulating substrates (Ta_3N_5/SiO_2). (a) Schematic depiction of RF magnetron sputtering process for the preparation of the precursor films on SiO_2 substrate. (b) schematic illustration of nitridation furnace under NH_3/N_2 mixed gas flow with the ratio of NH_3 : N_2 = 100 sccm : 100 sccm. (c) Temperature program for nitridation reaction under different nitridation temperatures (T) in the range from 725 °C to 850 °C.

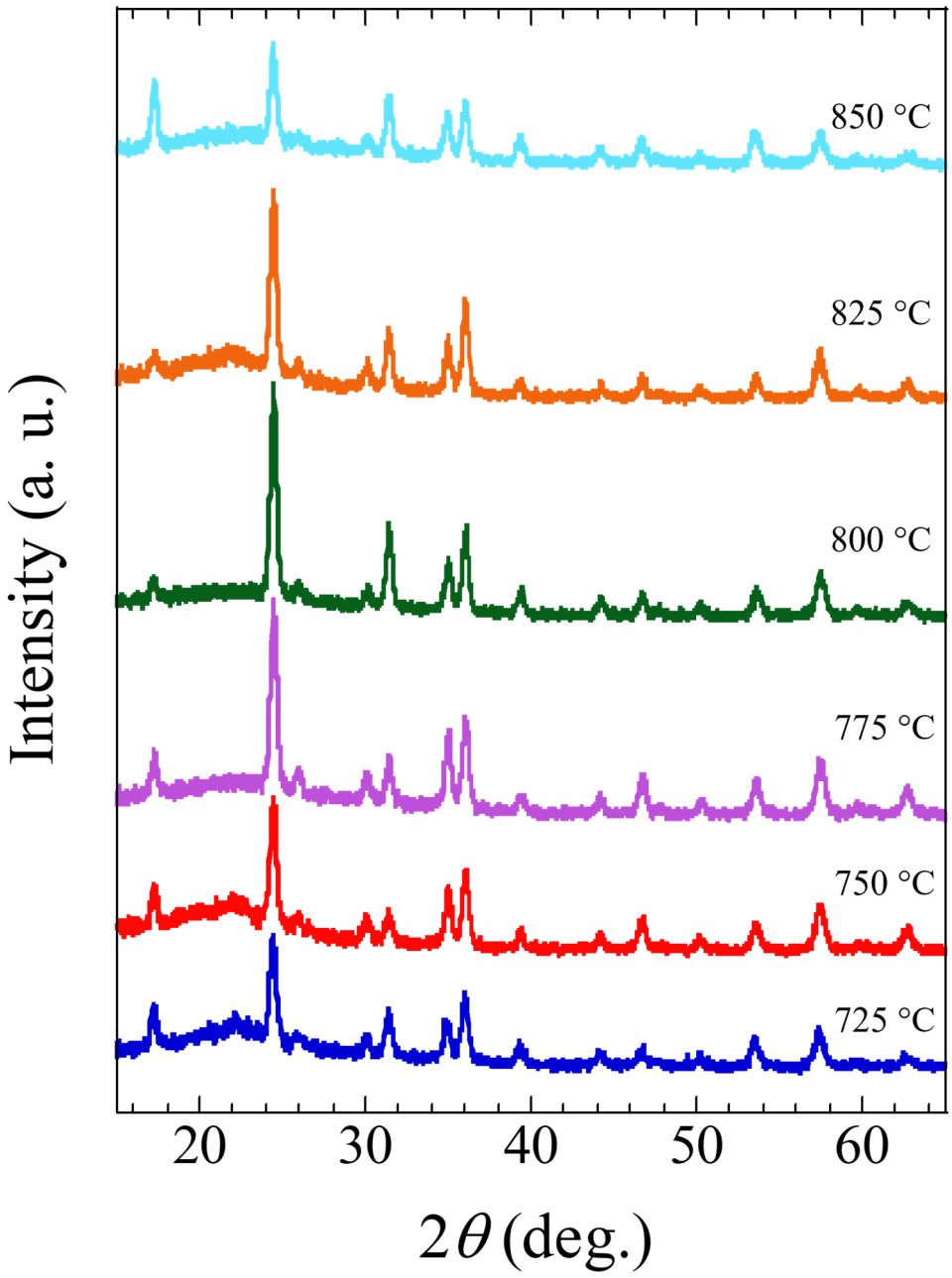

Figure S3. X-ray diffraction (XRD) patterns of Ta_3N_5/SiO_2 thin films prepared through the nitridation process with different temperatures (T) of 725, 750, 775, 800, 825, and 850 °C. The XRD patterns of all Ta_3N_5/SiO_2 samples can be assigned to a single phase of the monoclinic Ta_3N_5 material.

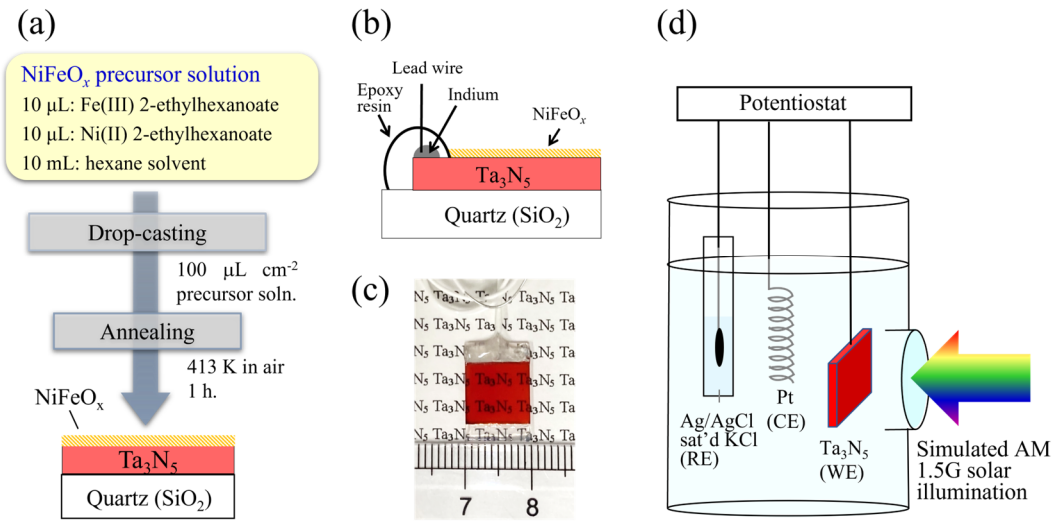

Figure S4. (a) Surface modification with $NiFeO_x$ electrocatalyst using a drop-casting method and thermal annealing on Ta_3N_5/SiO_2 thin film.[1] (b) Schematic and (c) photograph of $NiFeO_x/Ta_3N_5/SiO_2$ semitransparent photoanodes employed in a (d) three-electrode configuration for the photoelectrochemical (PEC) measurements.

Table S1. PEC properties of $NiFeO_x/Ta_3N_5/SiO_2$ thin films.

Nitridation temperature (°C)	J at 1.23 V_{RHE} (mA cm^{-2})	E_{on} (V_{RHE})	Maximum HC-STH (%)	Potential of maximum HC-STH (V_{RHE})
725	3.0	0.65	0.45	0.95
750	4.8	0.65	0.77	0.94
775	5.9	0.65	1.03	0.94
800	3.1	0.65	0.50	0.95
825	2.5	0.65	0.41	0.95
850	1.5	0.72	0.13	0.95

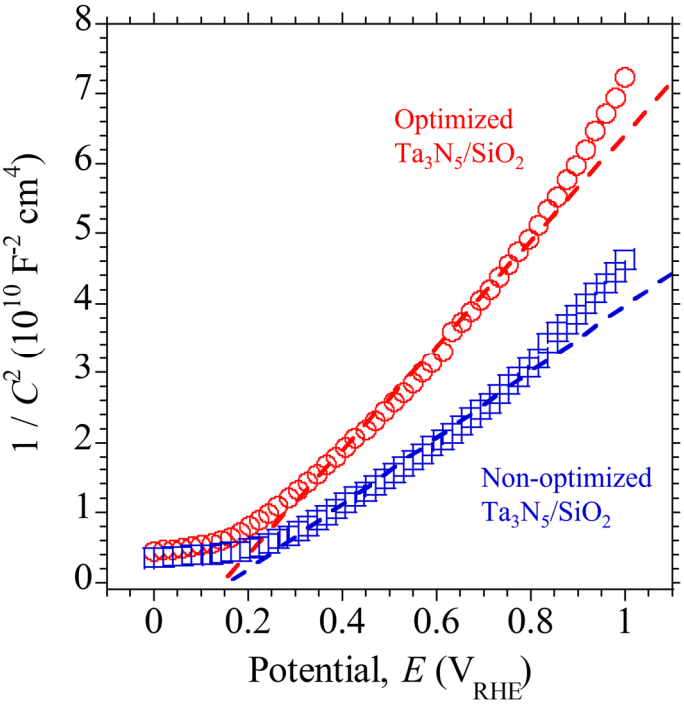

Figure S5. Mott-Schottky plots obtained from bare-Ta_3N_5/SiO_2 photoanodes at a potential modulation frequency of 1 kHz under dark conditions in 0.2 M potassium phosphate aqueous solution electrolyte (pH of 13, adjusted by KOH). The ac amplitude was 10 mV_{rms}. The carrier concentrations (N_d) of the optimized Ta_3N_5/SiO_2 (open circle colored in red) and the non-optimized Ta_3N_5/SiO_2 (open square colored in blue) were calculated to be 1.0×10^{20} cm^{-3} and 1.8×10^{20} cm^{-3}, respectively. To calculate the N_d values, the slope ranging from 0.8 V_{RHE} to 0.3 V_{RHE} (indicated by dashed lines) and the dielectric constant of 17 for the Ta_3N_5 were used.[3, 4]

Table S2. Electric properties of Ta_3N_5/SiO_2 thin films at room temperature

Nitridation temperature (°C)	Resistivity, ρ (Ω cm)	Carrier concentration, N_d (cm^{-3})	Hall mobility, μ_H ($cm^2\ V^{-1}\ s^{-1}$)	J at 1.23 V_{RHE} ($mA\ cm^{-2}$)
725	0.091	9.5×10^{19}	0.72	3.0
750	0.067	7.8×10^{19}	1.21	4.8
775	0.061	6.0×10^{19}	1.72	5.9
800	0.074	8.5×10^{19}	1.02	3.1
825	0.090	1.0×10^{20}	0.70	2.5
850	0.178	1.4×10^{20}	0.25	1.5

Table S3. Electric properties of Ta_3N_5-based photoelectrodes at room temperature.

Materials and substrates	Film thickness (nm)	ρ (Ω cm)	N_d (cm^{-3})	μ_H ($cm^2\ V^{-1}\ s^{-1}$)	J at 1.23 V_{RHE} ($mA\ cm^{-2}$)
Ta_3N_5/quartz[1*]	850	0.016	2.2×10^{20}	1.9	5.1
Ta_3N_5/quartz[2*]	1000	0.068	5.8×10^{19}	1.6	6.0
Ta_3N_5/FTO[3**]	115	1.43	2.31×10^{19}	0.19	2.4
Ta_3N_5/Ta-foil[4**]	960	0.45	4.7×10^{18}	2.9	0.16
Ta_3N_5 single crystal[5*]	—	5-8	$10^{18} – 10^{19}$	0.1 – 1.5	—
Ta_3N_5-NRs/Ta[6***]	600	—	3.7×10^{19}	—	4.0
Ta_3N_5 (100)-epitaxial/$LaAlO_3$[7*]	60	0.11	6.5×10^{19}	0.90	—
Ta_3N_5 (001)-epitaxial/$LaAlO_3$[7*]	60	0.045	2.5×10^{20}	0.54	—

*The data was acquired by Hall effect measurements at room temperature.

** Ta_3N_5 films were prepared on the quartz substrate using the same manner to fabricate the Ta_3N_5 on the conductive FTO and Ta-foil substrates.

*** The data were acquired by Mott- Schottky analysis.

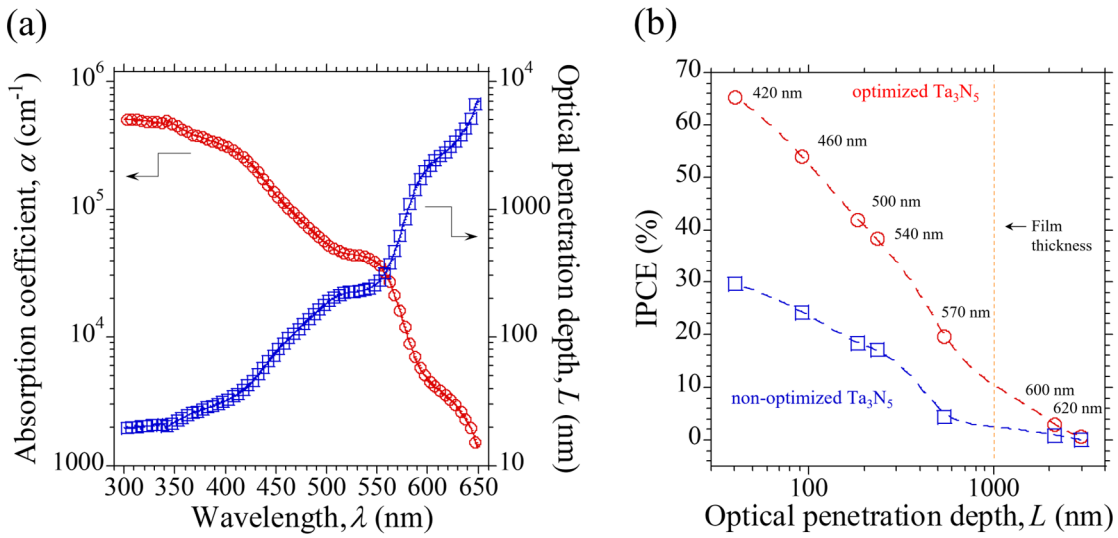

Figure S6. (a) Absorption coefficient (α) and optical penetration depth (L) of Ta_3N_5/SiO_2 thin films calculated from transmission/reflection spectrum of previously reported Ta_3N_5/SiO_2 with 200-nm-thick Ta_3N_5 film.[8] (b) Plot of IPCE values as a function of the L derived from the absorption coefficient spectra. The IPECs were obtained from the monochromatic light illumination at the wavelengths of 420, 460, 500, 540, 570, 600, and 620 nm.

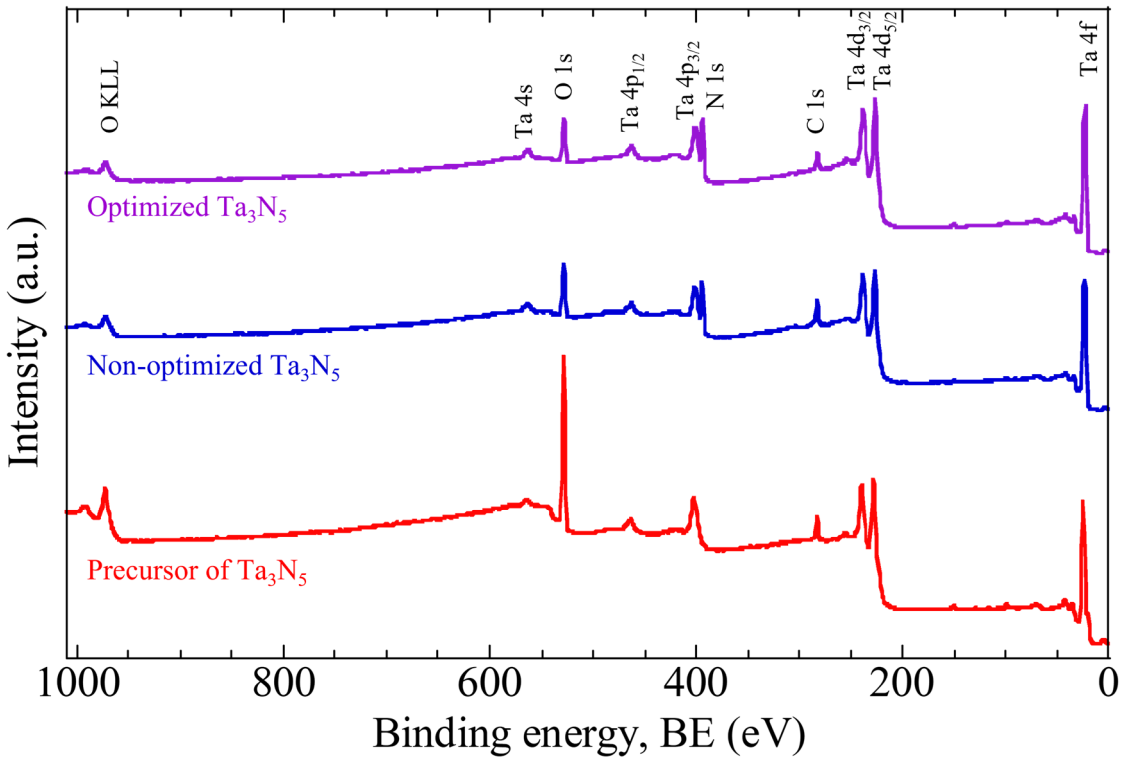

Figure S7. X-ray photoelectron spectroscopy (XPS) overall spectra of optimized Ta_3N_5/SiO_2, non-optimized Ta_3N_5/SiO_2, and precursor of Ta_3N_5/SiO_2 (Ta/SiO_2).

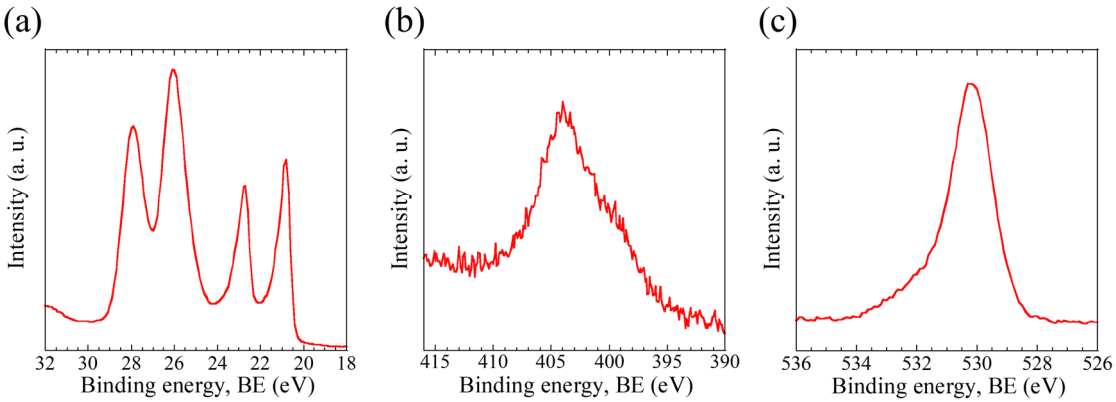

Figure S8. High-resolution XPS spectrum of mirror-polished Ta-metal plate as a reference, (a) Ta 4f, (b) Ta $4p_{3/2}$, and (c) O 1s.

(a)

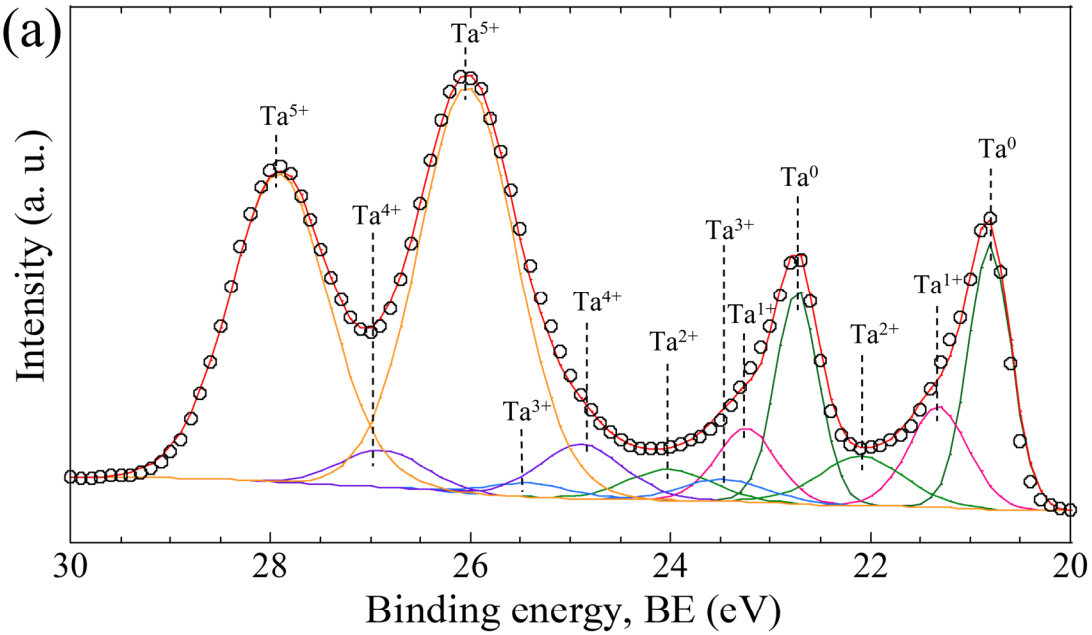

(b)

Sub oxide state of Ta	Ta 4f 7/2 (FWHM)	Ta 4f 5/2 (FWHM)
Ta^{0} (metal)	20.8 eV (0.50)	22.7 eV (0.50)
Ta^{1+} (Ta_2O)	21.3 eV (0.70)	23.2 eV (0.70)
Ta^{2+} (TaO)	22.1 eV (1.00)	24.0 eV (1.00)
Ta^{3+} (Ta_2O_3)	23.5 eV (1.00)	25.4 eV (1.00)
Ta^{4+} (TaO_2)	25.0 eV (1.00)	26.9 eV (1.00)
Ta^{5+} (Ta_2O_5)	26.0 eV (1.15)	27.9 eV (1.15)

Figure S9. XPS spectrum of Ta 4f peaks on mirror-polished Ta-metal plate with peak fitting curves (a) and XPS Ta 4f binding energies and full-width half-maximum (FWHM) in the peak fits for the spectrum (b).

Table S4. Surface concentration ratio of Ta, N, O elements on Ta_3N_5/SiO_2.

	Surface concentration ratio (%)		
	Ta / (Ta + N + O)	N / (Ta + N + O)	O / (Ta + N + O)
Optimized Ta_3N_5/SiO_2	33.7	43.4	22.9
Non-optimized Ta_3N_5/SiO_2	32.7	37.3	30.0
Precursor film (Ta/SiO_2)	31.7	—	68.3
Ta-metal plate (reference)	37.3	—	62.7

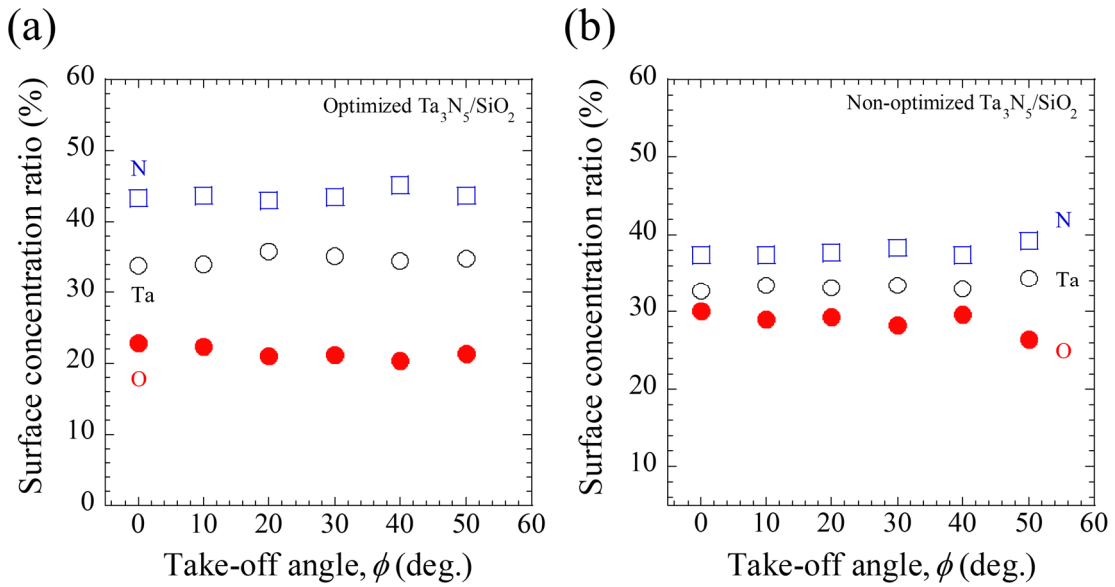

Figure S10. Surface concentration ratios of (a) optimized and (b) non-optimized Ta_3N_5/SiO_2 thin films evaluated through the results of AR-XPS analysis.

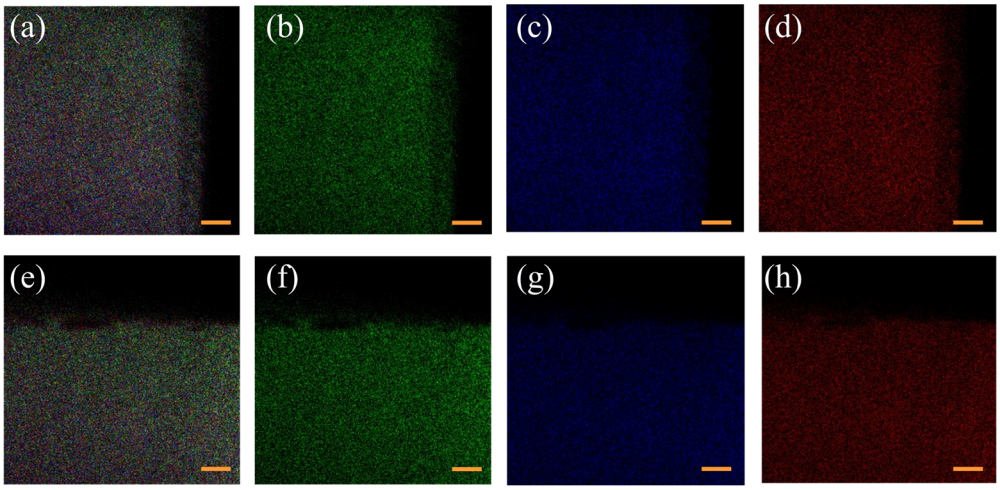

Figure S11. XPS-mapping for optimized Ta_3N_5/SiO_2 (a-d) and non-optimized Ta_3N_5/SiO_2 (e-h) thin films. (a and e) mixed map, (b and f) Ta $4f_{7/2}$ map, (c and g) N 1s map, (d and h) O 1s map. Scale bars (a-h) are 50 µm.

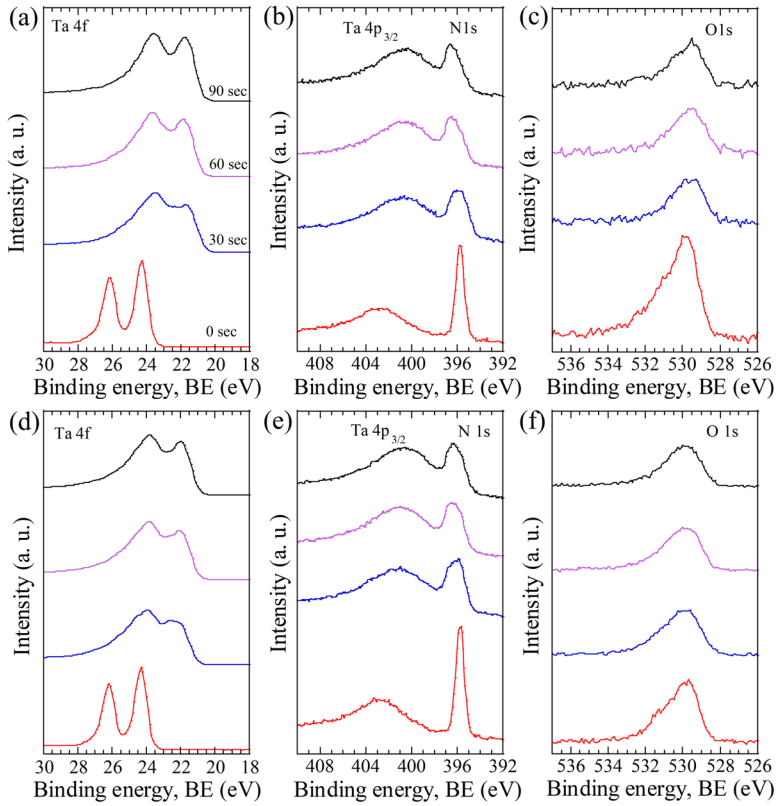

Figure S12. High-resolution XPS spectra after Ar-etching treatment over 0 sec (in red), 30 sec (in blue), 60 sec (in purple), and 90 sec (in black) of Ta_3N_5/SiO_2 thin films. The panels (a-c) and (d-f) correspond to XPS spectra of optimized Ta_3N_5/SiO_2 and non-optimized Ta_3N_5/SiO_2, respectively.

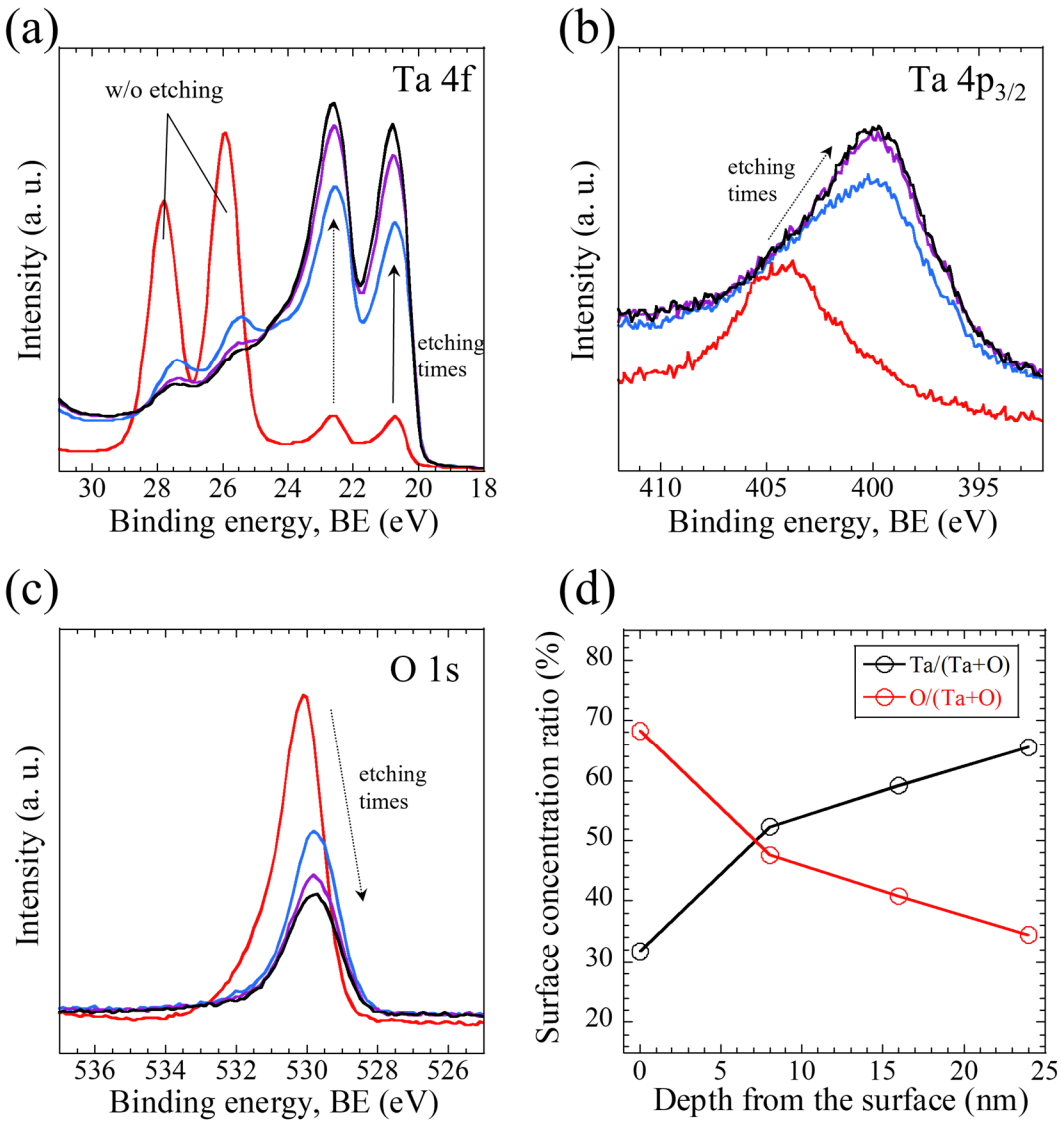

Figure S13. High-resolution XPS spectra of the precursor film (Ta/SiO_2) of Ta_3N_5/SiO_2 after Ar-etching treatment over 0 sec (in red), 30 sec (in blue), 60 sec (in purple), and 90 sec (in black). (a) Ta 4f, (b) Ta $4p_{3/2}$, (c) O1s. The arrows indicated the intensity of the XPS signal varies associated with repetitive Ar-etching. (d) Depth profile for surface concentration ratio of Ta and O on Ta/SiO_2.

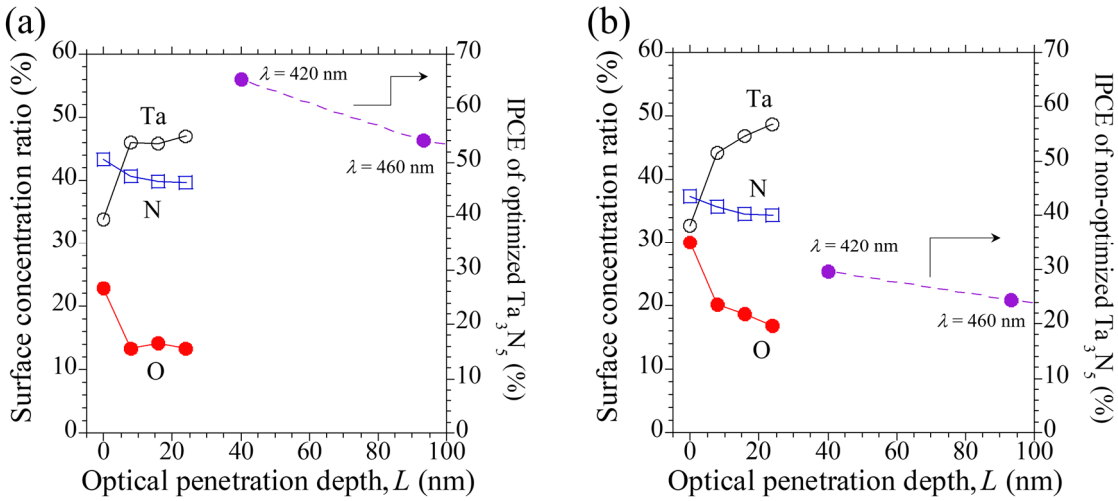

Figure S14. Plot of surface concentration ratio and IPCE values at 420 and 460 nm monochromatic light as a function of optical penetration depth (L) of the Ta_3N_5/SiO_2 thin film for optimized- (a) and non-optimized (b) samples. The L was calculated from the absorption coefficients of previously reported Ta_3N_5 thin film (Fig. S6).[8]

Table S5. Summary of PEC and electrical properties of Ta_3N_5/SiO_2

	J at 1.23 V_{RHE} (mA cm^{-2})	IPCE at 1.23 V_{RHE} at 420 nm (%)	σ (S cm^{-1})	N_d (cm^{-3})	μ_H (cm^2 V^{-1} s^{-1})
Optimized Ta_3N_5/SiO_2 processed at 775°C	5.9	65	16.4	6.0×10^{19}	1.72
Non-optimized Ta_3N_5/SiO_2 processed at 825°C	2.5	28	11.1	1.0×10^{20}	0.70

References

1. Y. Kawase, T. Higashi, M. Katayama, K. Domen and K. Takanabe, *ACS Appl. Mater. Interfaces*, 2021, **13**, 16317-16325.
2. T. Higashi, H. Nishiyama, Y. Otsuka, Y. Kawase, Y. Sasaki, M. Nakabayashi, M. Katayama, T. Minegishi, N. Shibata, K. Takanabe, T. Yamada and K. Domen, *ChemSusChem*, 2020, **13**, 1974-1978.
3. H. Hajibabaei, D. J. Little, A. Pandey, D. Wang, Z. Mi and T. W. Hamann, *ACS Appl. Mater. Interfaces*, 2019, **11**, 15457-15466.
4. A. Ziani, E. Nurlaela, D. S. Dhawale, D. A. Silva, E. Alarousu, O. F. Mohammed and K. Takanabe, *Phys. Chem. Chem. Phys.*, 2015, **17**, 2670-2677.
5. L. Jin, F. Cheng, H. Li and K. Xie, *Angew. Chem. Int. Ed.*, 2020, **59**, 8891-8895.
6. Y. Li, L. Zhang, A. Torres-Pardo, J. M. González-Calbet, Y. Ma, P. Oleynikov, O. Terasaki, S. Asahina, M. Shima, D. Cha, L. Zhao, K. Takanabe, J. Kubota and K. Domen, *Nat. Commun.*, 2013, **4**, 2566.
7. Y. Wang, Y. Hirose, T. Wakasugi, Y. Masubuchi, M. Tsuchii, Y. Sugisawa, D. Sekiba, A. Chikamatsu and T. Hasegawa, *J. Phys. Chem. Lett.*, 2021, **12**, 12323-12328.
8. T. Higashi, Y. Sasaki, Y. Kawase, H. Nishiyama, M. Katayama, K. Takanabe and K. Domen, *Catalysts*, 2021, **11**, 584.